Detailed Analysis of the Wake Structure of a Straight-Blade H-Darrieus Wind Turbine by Means of Wind Tunnel Experiments and Computational Fluid Dynamics Simulations

Alessandro Bianchini[1a], Francesco Balduzzi[2a], Giovanni Ferrara[3a], Lorenzo Ferrari[4b], Giacomo Persico[5c], Vincenzo Dossena[6c], Lorenzo Battisti[7d]

[a]*Department of Industrial Engineering, University of Florence, Via di Santa Marta 3, Firenze 50139, Italy*
[b]*Department of Energy, Systems, Territory and Construction Engineering, University of Pisa, Largo Lucio Lazzarino, Pisa 56122, Italy*
[c]*Dipartimento di Energia, Politecnico di Milano, Via Lambruschini 4, Milano 20156, Italy*
[d]*Department of Civil, Environmental and Mechanical Engineering, Universita di Trento, Via Mesiano 77, Trento 38123, Italy*

Darrieus vertical axis wind turbines (VAWTs) have been recently identified as the most promising solution for new types of applications, such as small-scale installations in com-plex terrains or offshore large floating platforms. To improve their efficiencies further and make them competitive with those of conventional horizontal axis wind turbines, a more in depth understanding of the physical phenomena that govern the aerodynamics past a rotating Darrieus turbine is needed. Within this context, computational fluid dynamics (CFD) can play a fundamental role, since it represents the only model able to provide a detailed and comprehensive representation of the flow. Due to the complexity of similar simulations, however, the possibility of having reliable and detailed experimen-tal data to be used as validation test cases is pivotal to tune the numerical tools. In this study, a two-dimensional (2D) unsteady Reynolds-averaged Navier–Stokes (U-RANS) computational model was applied to analyze the wake characteristics on the midplane of a small-size H-shaped Darrieus VAWT. The turbine was tested in a large-scale, open-jet wind tunnel, including both performance and wake measurements. Thanks to the avail-ability of such a unique set of experimental data, systematic comparisons between simu-lations and experiments were carried out for analyzing the structure of the wake and correlating the main macrostructures of the flow to the local aerodynamic features of the airfoils in cycloidal motion. In general, good agreement on the turbine performance esti-mation was constantly appreciated.

Introduction

The Darrieus concept is increasingly welcomed by both researchers and manufacturers of wind turbines, after most of the pilot research projects came to a standstill in the mid 1990s [1]. In particular, they are presently identified as suitable for new installation contexts such as complex or built terrains [2] or offshore floating platforms [3], thanks to some inherent advantages (independence on wind direction, generator positioned on the ground, low noise emissions, good performance in misaligned flows [4,5]).

Contributed by the Turbomachinery Committee of ASME for publication in the Journal of Engineering for Gas Turbines and Power. Manuscript received July 5, 2017; final manuscript received July 19, 2017; published online October 17, 2017. Editor: David Wisler.

[1]e-mail: bianchini@vega.de.unifi.it
[2]e-mail: balduzzi@vega.de.unifi.it
[3]e-mail: giovanni.ferrara@unifi.it
[4]e-mail: lorenzo.ferrari@unipi.it
[5]e-mail: vincenzo.dossena@polimi.it
[6]e-mail: giacomo.persico@polimi.it
[7]e-mail: lorenzo.battisti@unitn.it

At the present state of the art, however, the global efficiencies of Darrieus turbines still lack from those of horizontal axis wind turbines [1,6], due to their intrinsically more complex aerodynamics coming from the revolution of blades around an axis orthogonal to flow direction. To improve efficiencies further, a more in depth understanding of the physical phenomena that govern Darrieus turbine behavior is needed. Some of these phenomena, e.g., dynamic stall [7], flow curvature effects [8], and the impact of the Coriolis force on the blade boundary layer, are indeed not completely understood, and so limited corrections, or no correction at all, are applied for them when designing the rotors. Within this context, thanks to the rapidly increasing computational resources available; computational fluid dynamics (CFD) can play a fundamental role in enhancing the comprehension of the fluid structures

past these rotating blades, since it is the only model able to provide a comprehensive representation of the flow. Theoretically speaking, fully three-dimensional (3D) simulations would be required to describe the flow around these turbines: two-dimensional (2D) simulations indeed neglect the effect of the tip losses and of the struts and are deemed to produce vortices more coherent and less prone to breakdowns than actual ones. The present research on Darrieus vertical axis wind turbines (VAWTs) is indeed trying to move the CFD simulations toward fully three-dimensional analyses [9], which are however still hampered by the dramatic computational burden needed. On the other hand, recent studies (e.g., see Ref. [10]) showed that the approach here proposed, composed by a combination of 2D CFD simulations and empirical corrections, can give accurate estimates of the aerodynamics of these machines, even in terms of instantaneous torque profile. On these bases, the method is applied here to assess the main flow structures occurring in the wake of a H-Darrieus rotor [11]. Very few examples of similar activities are in fact presently known in the literature [12,13].

The availability of reliable and detailed experimental data is of major importance to tune the numerical tools, especially for VAWTs, whose aerodynamics involve inherent unsteady flows and, in most configurations, flow detachment phenomena. Within this framework, a comprehensive experimental research program on VAWTs has been carried out in the recent past by the University of Trento and the Politecnico di Milano, in the frame of a national founded project. Part of the results of this study is documented in Refs. [14] and [15]. In the project, two rotor architectures (closed-troposkien-blade and open-H-blade) were tested in several flow conditions, measuring both the overall performance and the wake velocity profiles, in view of creating a benchmark for validation of theoretical models. Making use of such a unique experimental database, this paper presents a systematic comparison between the experimental results of the H-shaped rotor at the midplane and the numerical simulations coming from a two-dimensional unsteady Reynolds-averaged Navier–Stokes (U-RANS) computational model, developed by some of the authors in the last few years [10]. The main scope of this comparison is to analyze the shape of the wake and to correlate the main macrostructures of the flow to the aerodynamics of the airfoils in cycloidal motion.

Turbine Layout

The model used during the experimental tests, depicted in Fig. 1, is a three-blade, H-Darrieus turbine. The turbine has a swept area of 1.5 m^2 ($H \times D$, 1.46 m × 1.03 m), and it is equipped with dihedral blades composed by unstaggered NACA0021 profiles featuring a chord $c = 0.086$ m. Additional details on the rotor model are reported in Ref. [14].

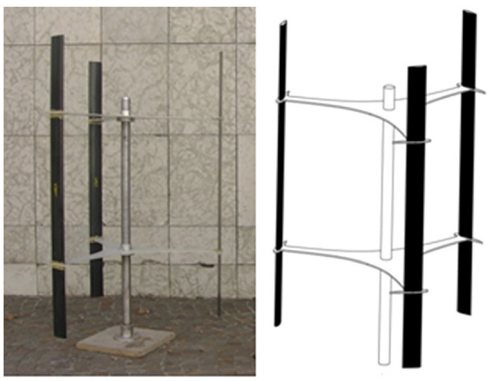

(*a*) (*b*)

Fig. 1 Picture (*a*) and design sketch (*b*) of the tested H-Darrieus VAWT

Experimental Campaign

The aerodynamics and performance of the VAWT model were investigated in detail in dedicated wind tunnel experiments performed by some of the authors in a recent test campaign, widely documented in Ref. [14]. In the frame of this experimental activity, mechanical measurements on the shaft as well as velocity measurements in the wake downstream of the rotor were carried out. Only a brief review of the experimental approach is reported here, while full details on the test campaign can be found in Ref. [14].

Wind Tunnel. The measurements reported in this paper were performed in the large-scale wind tunnel of the Politecnico di Milano, Milano, Italy. It consists of a closed-loop facility, whose test section (4.00 m wide, 3.84 m high, and 6.00 m long) allows the aerodynamic characterization of real-scale wind turbines for microgeneration (within 1 kW). A combination of honeycombs and antiturbulence screens provides high flow quality, resulting in freestream turbulence intensity at the inlet lower than 1%.

Since the solid blockage in confined environment would have been about 10% of the wind tunnel chamber, tests were carried out using a "free jet" (or "open chamber") configuration, by removing the test room and installing the rotor directly facing the upstream tunnel. Application of classical correlations for free-jet blockage suggests that the blockage is negligible in the present case (about 1.5%) [14]; therefore, free-jet wind tunnel results can be considered representative of the open field configuration.

Instrumentation and Data Processing. The experimental turbine performance was obtained by combining an absolute encoder (for rotational speed measurements) and a precision torque meter (to measure the torque transmitted through the shaft). Data were registered using a Compact-RIO (National Instruments, Austin, TX) data acquisition board, setting a sampling frequency of 2 kHz for time series of 3 min, to achieve a sufficient amount of data for time-averaging. Measurement uncertainty was computed by resorting to the classical error propagation theory; the reader is referred to Ref. [14] for the quantification of the uncertainty as a function of the tip-speed ratio (TSR). The resulting uncertainty values are explicitly reported in the form of error bars, when plotting the performance curve of the VAWT in the Results section.

To measure the velocity magnitude and the turbulence intensity in the wake, two single-sensor hot wire probes were traversed downstream of the rotor. Uncertainty in the velocity measurements resulted in about 2% after calibration in a low-speed jet. The first hot wire probe was mounted aligned with the wind speed direction, thus exposing the wire normal to the wind to measure directly the velocity magnitude. The second probe was mounted in the vertical direction and was rotated during operation around its own axis to measure the flow direction. The so-called "triple decomposition" was performed on hot wire data, by extracting the time-averaged, phase-resolved, and turbulent components of the velocity, as discussed in Ref. [15]. The phase-resolved component was obtained by ensemble averaging the velocity signals, using the encoder as a key-phasor. The streamwise turbulence intensity was determined by extracting the unresolved unsteady fluctuations of the velocity signal. A pneumatic five-hole probe was also applied throughout the tests to measure the pressure level and the 3D flow direction. Measured pressure values confirmed the absence of blockage-induced over-speeds outside the wake region; flow angle measurements with the vertical hot wire and the pneumatic probe also indicated negligible transversal and vertical velocity components in the wake at midspan.

Computational Fluid Dynamics Simulations

This study made use of two-dimensional unsteady CFD simulations, based on the Reynolds-averaged Navier–Stokes equations (U-RANS). The main issue in using such an approach is that these

simulations can be deemed to produce vortices that are more coherent and less prone to breakdowns than real 3D ones. However, recent studies [11,16–19] have shown that the 2D U-RANS approach can provide accurate estimations of the performance and can even provide a realistic description of the flow field around the blades.

In further detail, the simulations presented in this paper were carried out using the commercial code ANSYS FLUENT [20] using the pressure-based formulation for solving the Navier–Stokes equations. The fluid was air, which was modeled as an ideal compressible fluid following the suggestion of Balduzzi et al. [10], who proved that the local accelerations on the airfoils can be predicted more accurately by the compressible formulation. Inlet air conditions were imposed equal to those monitored during the experimental tests, i.e., a pressure of 1.01×10^5 Pa, a temperature of 293 K and an inlet turbulence level of 1%. The assessment and validation of the main settings for a proper CFD simulation of Darrieus wind turbines using the FLUENT code have been recently presented by Balduzzi et al. [10,21,22], and the accuracy of the approach has been also successfully verified by means of the experimental data [10,23,24].

For the sake of completeness, the main numerical settings are, however, briefly summarized. The turbulence closure was achieved by means of the k–ω shear stress transport model [25], coupled with the enhanced wall treatment embedded in the FLUENT code. The coupled algorithm was preferred to handle the pressure–velocity coupling. The second-order upwind scheme was used for the spatial discretization of the Reynolds-averaged Navier–Stokes and turbulence equations, as well as the bounded second order for time differencing to obtain a good resolution [26]. The global convergence of each simulation was monitored by considering the difference between the mean values of the torque coefficient over two subsequent revolutions; according to Ref. [10], the periodicity error threshold was set to 0.1%. To simulate the rotation of the turbine, the sliding mesh technique was employed, i.e., the computed domain was split into a circular zone containing the turbine, rotating with the same angular velocity of the rotor, and an outer rectangular fixed zone, determining the overall domain extent. The final dimensions of both domains were defined following the sensitivity analysis reported in Ref. [10], so as to allow a full and unconstrained development of the turbine wake [16] and make simulations properly comparable to the experiments obtained in an unconfined configuration [14]. The selected boundary conditions were: (a) a velocity-inlet condition at the inlet section (40D upwind from the revolution axis), (b) the ambient pressure condition at the outlet boundary (100D downwind), and (c) a symmetry condition on lateral boundaries (30D).

The mesh (details are reported in Fig. 2) is of unstructured and hybrid type, with triangular elements in the core flow region, and an O-grid made of quads in the boundary layer regions. The first element height was chosen to guarantee that the dimensionless wall distance at the grid nodes of the first layer above the blade wall does not exceed the limit of $y^+ \sim 1$. The expansion ratio for the growth of elements starting from the surface was kept below 1.1 to achieve good mesh quality [10]. A mesh sensitivity analysis was carried out to guarantee a fully grid-independent behavior. The complete results of the sensitivity analysis are reported by Balduzzi et al. [10,22]. Six different levels of refinement of the mesh and three angular time-steps were tested to ensure an adequate spatial discretization level, using the number of grid nodes past the airfoil as the driving parameter for varying the grid size. Grid-independent results were achieved when adopting more than 700 nodes on the airfoil surface for the high tip-speed ratios (TSR > 2.6), while the number of nodes required at low TSRs is almost doubled. A negligible difference in the average torque prediction (lower than 0.8%) was observed between the two most refined grid levels investigated.

In this study, the airfoil surface was discretized with 1400 nodes for all the investigated regimes, corresponding to the finest mesh defined during the sensitivity analyses reported in Ref. [22]. Even though redundant, this refinement level indeed ensured a very accurate discretization of the whole area around the rotor, limiting the bias error due to the numerical discretization. As a result, the computational grid was characterized by 1.2×10^6 elements in the rotating region and 2.0×10^5 elements in the stationary region. Overall, the mesh characteristics fully accomplish the criteria based on dimensionless thresholds proposed in Ref. [21]. Based on the same criteria, in order to limit the Courant number in proximity of the blades, an angular timestep of 0.21 deg was used. With the aforementioned settings, the calculation time to achieve a complete revolution of the rotor was around 24 h in a 16 CPUs (2.8 MHz each) calculation center. The required number of

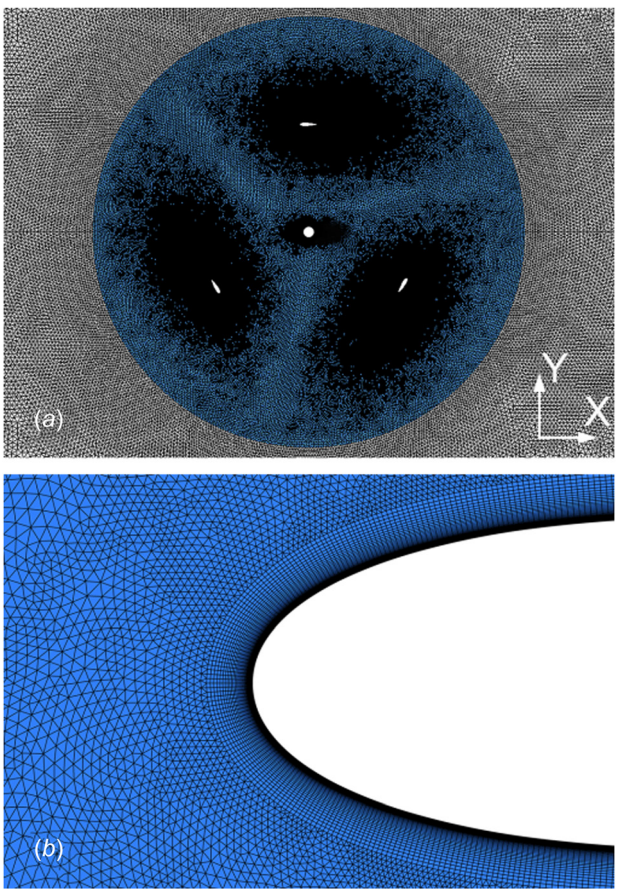

Fig. 2 Mesh refinement in the rotating region (*a*) and near the leading edge (*b*)

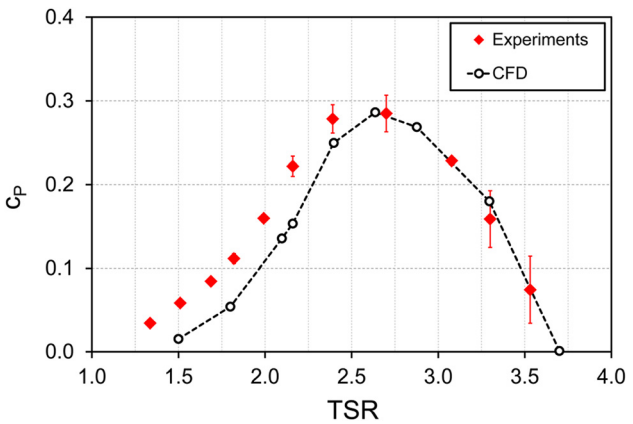

Fig. 3 Power coefficient versus TSR: comparison between experiments [14] and simulations

revolutions to achieve a periodic solution is dependent on the TSR [10], varying from 15 to 25 revolutions.

Results

Power Curve. The prediction capabilities of numerical simulations were first assessed in Fig. 3 comparing the calculated and the experimental [14] curves of the power coefficient

$$c_P = \frac{P}{\frac{1}{2}\rho A {V_0}^3} \tag{1}$$

In order to properly compare the data, numerical results in the figure were corrected a posteriori to account for two of the main parasitic effects affecting the performance of a Darrieus VAWT, i.e., the resistant torque of the supporting spokes and the tip effects. Indeed, both these sources of torque loss could not be included in a two-dimensional simulation approach.

The correction was introduced by resorting to the original lumped-parameters model developed in Ref. [27]. The model makes use of the blade element momentum multitubes approach for the discretization of the rotor.

With reference to Fig. 4, for each revolution speed, Ω, the normal component of the relative velocity on the struts $W_\perp$ (i.e., the one really producing drag [28]) is evaluated at a discrete number of positions O_j as a function of the approaching wind velocity, U'_θ (reduced by the induction factor), the azimuthal position and the local radius, R_j. The equivalent drag coefficient is dependent on the struts cross section. Based on these hypotheses, the average parasitic torque of a rotating strut at a given Ω is given by Eq. (2), where C_A is the equivalent chord of the strut [27]. For further details on the model, the reader has referred to the analyses of Bianchini and coworkers [16] and [22], where the reliability of the model was assessed by means of the experimental tests in the wind tunnel. In addition, numerical results were further processed to account for tip-losses. To this end, the results of a recent high-computing 3D study [9] were exploited. The cited work was carried out on a single blade equal to one of those used in the present experiments. The authors found that the tip flow effects adversely affect the performance for a span length of approximately 2.6c from each tip. The overall performance deficit in terms of produced torque in comparison to the infinite-wing was then estimated in an equivalent blade span reduction of 1.5c, i.e., the produced torque is equal to that produced by a similar blade shorter by 1.5c. This result—used here to correct the power curve—was also found in good agreement with the reduction estimated by the Leicester–Prandtl model [1] that is commonly used, for example, in blade element momentum codes to account for tip effects. Upon examination of Fig. 3, sound agreement between simulations and experiments can be appreciated. Simulations were indeed able to describe the power curve over the entire range of TSRs, both in terms of qualitative trend and of c_P values. As discussed in Ref. [11], a little discrepancy is only noticeable at low tip-speed ratios

$$T_{\text{res}}(\Omega) = \frac{1}{4\pi}\rho C_A \int_0^{2\pi}\int_{D_T/2}^{R} C_D(\Omega,\theta,R)\cdot W_\perp(\theta,R)^2 dR d\theta \tag{2}$$

Based on the analyses reported in Refs. [1] and [10], in this region of the curve, the airfoils indeed work in stalled conditions for a considerable fraction of the revolution, with severe flow separation phenomena and macrovortices detaching from the airfoils. In these conditions, additional factors like the surface roughness, the trailing-edge refinement in the experimental model, the inherent limitations of turbulence models in predicting highly separated flows, etc., can then play a fundamental role in setting the characteristics of such separations, which are however pivotal for the final torque production. By virtue of these results, the CFD approach was considered reliable for the purposes of this study.

Mean Wake Profiles. The mean velocity profiles within the wake of the turbine are first analyzed. To facilitate the reader during the discussion of the results, Fig. 5 displays the convention on signs and reference axes considered for the rotor. CFD data have been acquired in correspondence of a virtual rake positioned exactly at the same distance from the shaft of the experimental "near" traverse, i.e., 0.75D downstream of the shaft. At this section, 100 equally spaced points were acquired at a frequency of 10 kHz for ten complete revolutions. In a previous study [11], the same authors analyzed the evolution of the wake as a function of the tip-speed ratio. The results highlighted that in the left-hand side of the operating curve (i.e., the stable one) the wake shape is very smooth and no particular macrostructures can be identified in the flow. For example, Fig. 6 reports the dimensionless velocity (V/V_0) profile in the wake at TSR = 3.3.

In the following, the focus of the analysis is then reserved to the unstable part of the curve, with the aim of correlating the main flow structures recognized by the wake profile to the unsteady aerodynamics of the airfoils. To this end, Fig. 7 first reports the

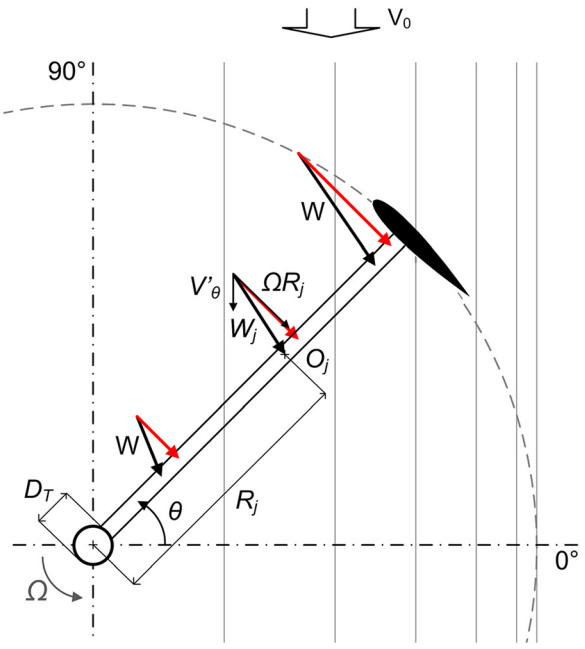

Fig. 4 Model for the calculation of the resistant torque of the struts

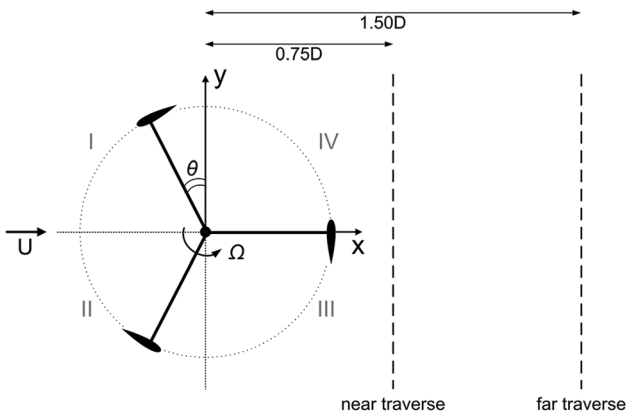

Fig. 5 Signs and conventions for the analysis

results relative to three relevant tip-speed ratios, namely TSR = 1.5, TSR = 1.8, and TSR = 2.4.

These functioning conditions correspond to a condition with very low torque, the first inflection point of the curve, and a near-peak condition, respectively. More specifically, in the left-hand side of the figure comparisons were again made between the numerical results and the experiments in terms of time-averaged profiles of dimensionless velocity (V/V_0) in the near traverse, i.e., 0.75D downstream of the shaft. In the right-hand side of the figure, instantaneous snapshots of the dimensionless velocity fields are also reported for the same azimuthal position of the blade. These flow field visualizations, even if referred only to a specific instant in time, are indeed useful to highlight some relevant aerodynamic structures. Upon examination of the results, a satisfactory agreement is noticeable between measured and computed wake profiles, with a better matching at lower tip-speed ratios.

This result is apparently in contrast with the results of Fig. 3, where the accuracy is poorer at lower TSRs. The main issue in correctly predicting the operation near the peak power relies, however, in the fact that the overall power production is mainly dependent on the correct description of the stall characteristics of the airfoils in the upwind region of the rotor (i.e., $0\,\text{deg} < \theta < 180\,\text{deg}$), which is particularly critical in CFD analyses as discussed before. According to Ref. [11], at TSR = 2.4 a discrepancy can be also noticed in the region behind the rotor, where experiments revealed a velocity deficit higher than that predicted numerically. Such deviation might be connected to a higher impact of the interaction between the flow and the tower. This evidence is in agreement with the slightly lower value of the predicted power coefficient previously discussed in Fig. 3.

By looking at the velocity fields, the increase of the wake coherence as a function of the tip-speed ratio is evident. At the two lowest TSRs, the velocity pattern within the wake presents high gradients and shows the propagation of strong vortices, which remarkably affects the performance of the rotor. The strongest vortices are generated by the deep stall experienced by the airfoils in the upwind region [29,30].

An additional ripple (located approximately behind the tower) is instead connected to another set of vortices that originate from the airfoil leading edge as soon as the incidence angle is decreasing again toward values which allow the flow to reattach to the blades. This latter phenomenon is particularly intense at TSR = 1.8, inducing a non-negligible energy recovery in the mid of the wake.

To further comprehend its nature, Fig. 8 reports the evolution of the velocity field behind the tower for six relevant azimuthal positions. Upon examination of the figure, one can notice that, as soon as the incidence on the airfoils starts redecreasing toward values for which the flow is able to stay attached to the airfoil, a set of vortices is detached by the leading edge of the blade. These vortices are then convected downstream by the main flow, generating the local velocity increments revealed by the data measured at the near traverse.

It is worth noticing that, for all of the analyzed TSRs, the wake profiles are fairly similar in the advancing-blade half of the domain (positive Y), but they are substantially different in retreating-blade half of the domain (negative Y). Indeed, at TSR = 1.5 the velocity deficit is strongly asymmetric due to a sudden decrease of the energy extraction in the leeward side of the turbine. Conversely, at TSR = 2.4, the wake shape is rather symmetric, with a steep reduction of velocity occurring both at $Y/D = 0.5$ and $Y/D = -0.5$. The condition at TSR = 1.8 shows several flow features comparable to what is seen for both TSR = 1.5 and TSR = 2.4. Indeed, a sudden decrease of energy extraction between $-0.2 < Y/D < 0.0$ can be noticed, as well as a steep reduction of velocity at $Y/D = -0.5$.

To correlate the previously discussed details of the wake structure to the aerodynamic behavior of the blades, the evolution of the flow filed around the blades is analyzed in detail. Figures 9 and 10 show the vorticity field in the near blade region at various blade azimuthal positions. The three relevant tip-speed ratios (TSR = 1.5, TSR = 1.8, and TSR = 2.4) are compared in the figures. The vorticity is reported in a dimensionless form (ω^*), normalized by the freestream velocity and the blade chord as in the below equation:

$$\omega^* = \frac{\dfrac{dV_y}{dx} - \dfrac{dV_x}{dy}}{V_0 \cdot c} \tag{3}$$

The stall evolution in the upwind part of the rotation reported in Fig. 9 reveals that the vortices are shed from the blade around the position of $\vartheta = 90\,\text{deg}$ for both TSR = 1.5 and TSR = 1.8, while the wake is stable for TSR = 2.4. This phenomenon explains why the location of maximum velocity deficit lies between $-0.2 < Y/D < 0.0$ at TSR = 2.4, while lower TSRs are characterized by strong localized regions of fluctuations in the wake. Conversely, the aerodynamic behavior in the third quadrant at TSR = 1.8 is closer to that at TSR = 2.4, as shown in Fig. 10. It is observed that the flow reattaches to the blade beyond $\vartheta = 180\,\text{deg}$, thus promoting the energy extraction noticeable upon examination of the profiles reported in Fig. 7. Finally, at TSR = 1.5, the blade still suffers from large separated regions and from the onset of vortices taking place at the leading edge.

Wake Unsteadiness. The analysis of the complex flow fields predicted in the wake, dominated by the alternate passage of macrovortices, corroborates the conclusion of Persico and coworkers [14] that the unsteadiness may have a remarkable impact on the flow behind a H-Darrieus rotor like the one investigated here, especially at low TSRs. From this perspective, the averaged wake profiles described before in the paper may not be sufficient to fully describe the attended conditions behind the rotors.

To quantify the variability of the wake due to unsteadiness, the experimental data were further processed by calculating the "periodic unsteadiness" of the wake velocity profile, defined as the root mean square of the phase-resolved velocity component (locked at the turbine revolution frequency) and expressed as percentage of the undisturbed wind speed. In further detail, the phase-resolved velocity component was first calculated (Eq. (4)) as the ensemble average among values acquired at the same phase (index j) for all the different revolutions acquired (index i) purged of the time-mean value

$$V_{\text{PER}}(j;X,Y) = \frac{\sum_{i=1}^{N_{BPP}} \left(V(i,j;X,Y) - V_{TM}(X,Y)\right)}{N_{BPP}} \tag{4}$$

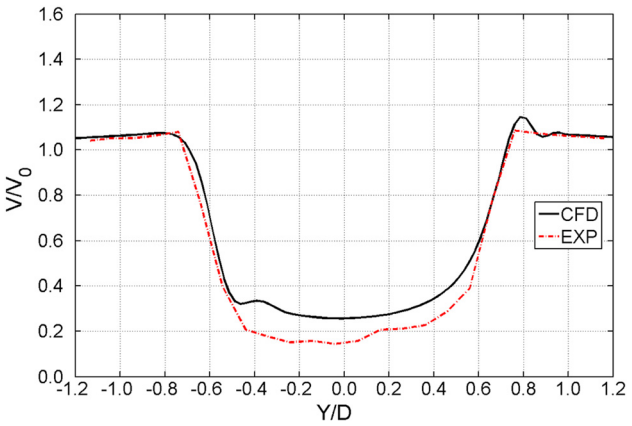

Fig. 6 Dimensionless velocity in the near traverse at TSR = 3.3: CFD versus experiments

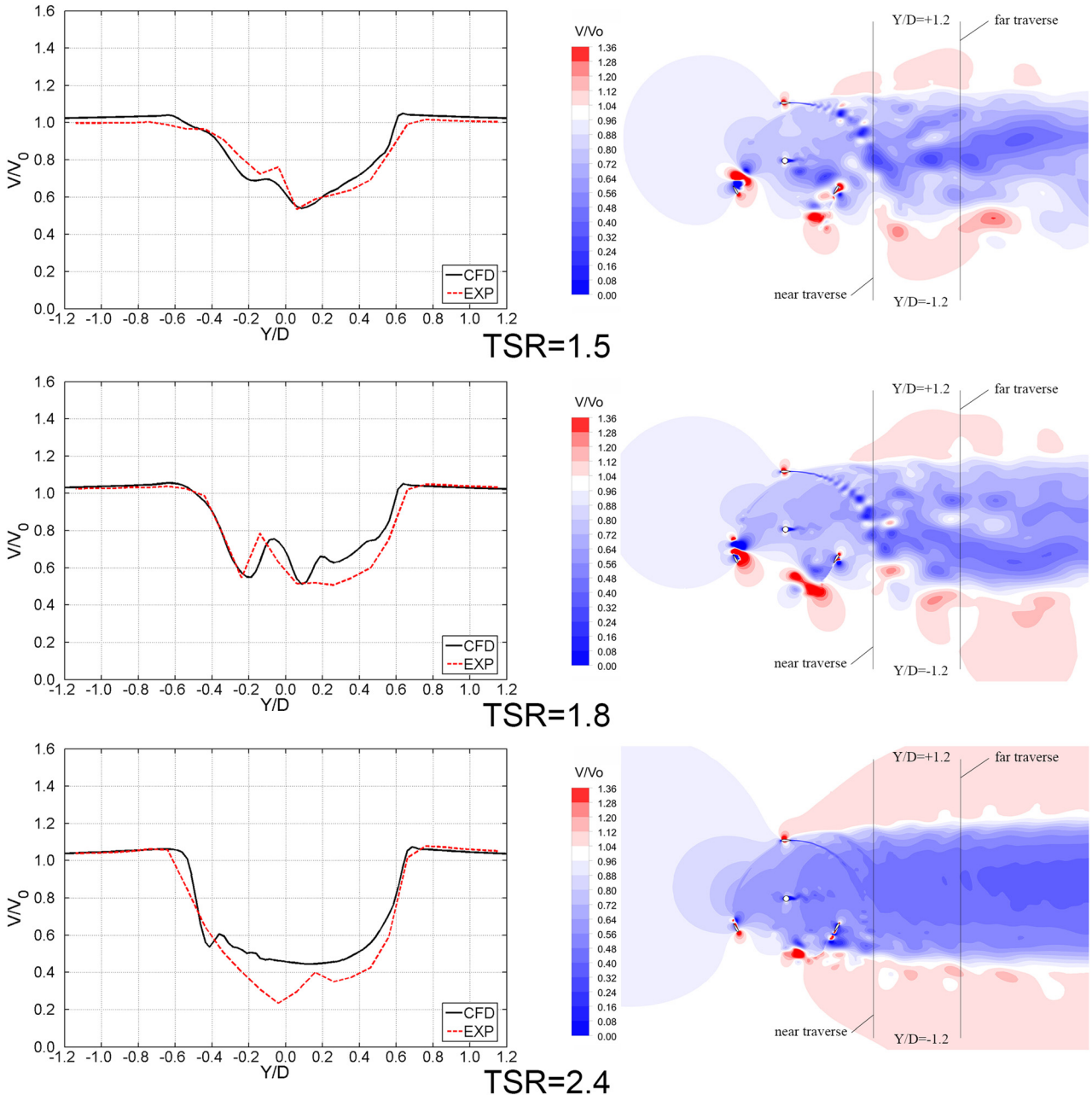

Fig. 7 Wake analysis in the near traverse at TSR = 1.5, TSR = 1.8, and TSR = 2.4. Right: comparison of computed mean wakes profiles—in terms of dimensionless velocity—between CFD and experiments. Left: instantaneous contour plots of dimensionless velocity in the same azimuthal position of the rotor.

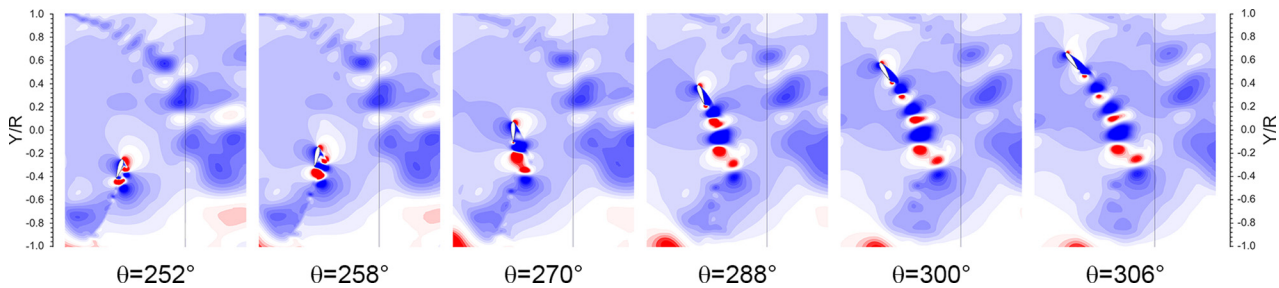

Fig. 8 Velocity distribution at TSR = 1.8 around $\theta = 270$ deg (dimensionless velocity contours reported with the same scale of Fig. 7)

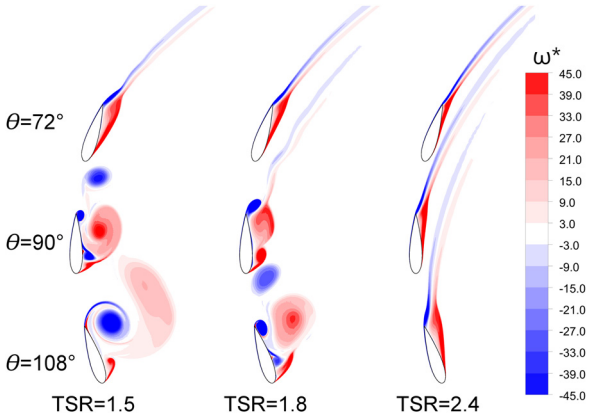

Fig. 9 Contour plots of dimensionless vorticity around $\theta = 90$ deg

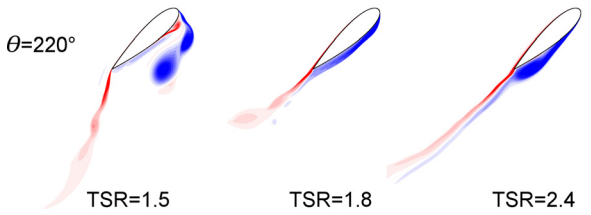

Fig. 10 Contour plots of dimensionless vorticity at $\theta = 220$ deg (same scale of Fig. 9)

The root mean square of the periodic velocity component I_{PER} was then calculated to extract the synthetic information on the wake character by the below equation:

$$I_{PER}(X,Y) = \sqrt{\frac{\sum_{j=1}^{N_{PER}} (V_{PER}(j;X,Y))^2}{N_{PER}}} \quad (5)$$

The same data processing method was also applied to the CFD simulations for the three relevant TSRs of Fig. 7. To highlight the impact of periodic unsteadiness on the wake profile, Fig. 11 reports the I_{PER} values for TSR = 1.5 as variation bars superimposed to the mean wake profile. The periodic unsteadiness indeed represents the variability of the wake profile in different revolution cycles of the turbine. To improve the clarity of the figure, periodic unsteadiness for the CFD data has been displayed only in correspondence to the Y/D values for which experimental data were available.

Sound agreement between experiments and CFD can be readily noticed in terms of magnitude and distribution of the periodic unsteadiness.

Upon additional examination of the figure, it is also apparent that

- as one may expect from the flow field analyses of Fig. 7, higher unsteadiness is noticed in the wake between $Y/D = -0.7$ and $Y/D = 0$, i.e., where the macrovortices are being detached from the blades and convected downstream by the main flow, as a result of the severe incidence angle fluctuations experienced by the airfoils in this region.
- in this region, the wake shape is strongly unsteady, resulting in a pulsating flow which is believed to be detrimental for a downstream rotor.

The trends of periodic unsteadiness were then calculated for all the available TSRs and reported in Fig. 12.

Even though inherent potential limitations might affect the U-RANS approach (e.g., due to a not fully reliable description of the vortex propagation, in comparison, for example, to a large eddy simulation approach), a very significant matching was obtained between numerical simulations and experimental data, both in terms of computed unsteadiness values and of their distribution along the wake.

The profiles, again reported for the near traverse, confirmed the former observations based on the analysis of the instantaneous velocity fields, highlighting a larger presence of unsteadiness in the negative Y/D positions and in the center of the wake, where the vortices' passage is more intense.

Moving from low TSRs to those located in the stable part of the operating curve, the unsteadiness is remarkably reduced (almost

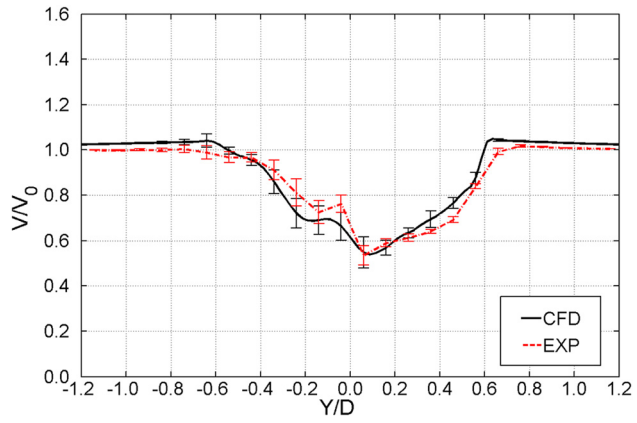

Fig. 11 Mean wake profiles and periodic unsteadiness at TSR = 1.5: comparison between CFD and experiments

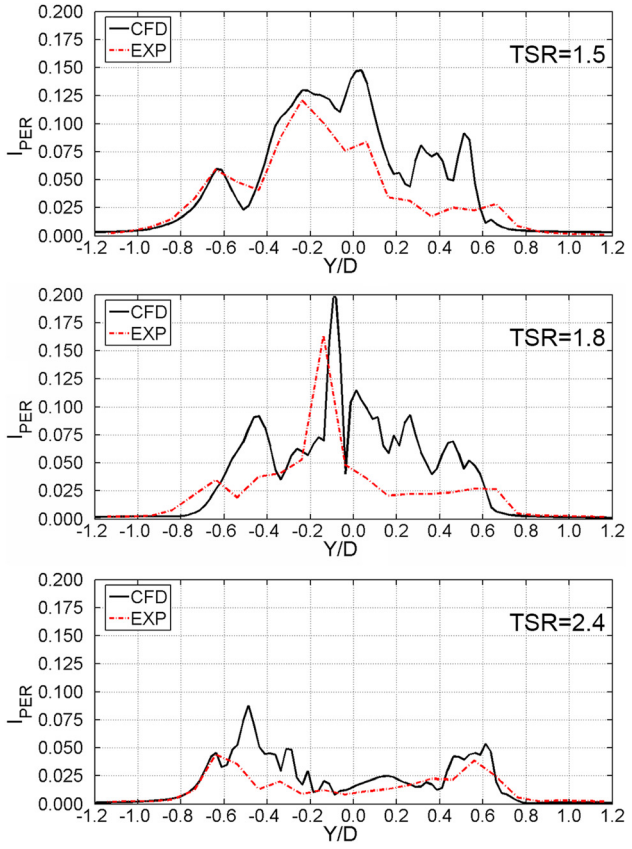

Fig. 12 I_{PER} values for three relevant TSRs: comparison between CFD and experiments

halved). The central increment due to the passage of vortices is reduced and higher values are shifted toward the external boundaries of the wake, where the shear layer between the turbine wake and the undisturbed flow undergoes residual oscillations.

Conclusions

In this paper, a comprehensive set of flow measurements in the midplane inside the wake of a H-Darrieus vertical-axis wind turbine has been used as a benchmark for comparison with two-dimensional U-RANS CFD simulations. The purpose of the study was, in particular, to analyze the main flow macrostructures in the wake and to try correlating them with the aerodynamics of rotating airfoils.

Overall, an interesting and significant agreement was found between measurements and U-RANS simulations. In particular, CFD data have been shown to provide reliable predictions of the turbine performance and also to reproduce most of the flow structures featuring the midspan section of the wake, whose effects appear fully compatible with experimental trends.

Special attention was particularly paid to the tip-speed ratios in the unstable part of the power curve, where the wake has been shown to be characterized by very intense ripples, due to the passage of macrovortices detaching from the blades either in the upwind region after the stall angle is reached, or in the downwind region (i.e., $180\,\text{deg} < \theta < 360\,\text{deg}$) as soon as the flow tends to re-attach to the blade. Phase-resolved data further showed that substantial agreement was achieved also in terms of periodic unsteadiness of the wake.

According to the higher data dispersion noticed in time data and to the analysis of the computed flow fields for the lower TSRs, the wake unsteadiness is particularly evident in all those zones affected by the vortices' passage, resulting in a pulsating wake, which is thought to be potentially detrimental, for example, for a downstream rotor.

Acknowledgment

Thanks are due to Professor Ennio Antonio Carnevale of the University of Florence for supporting this study, and to Dr. Andrea Tanganelli for his contribution to CFD simulations.

The authors would like also to acknowledge the company Tozzi-Nord Wind Turbines for the rotor model and the technicians and collaborators of the Università di Trento and the Politecnico di Milano for their precious support before and during the tests.

Nomenclature

A = turbine's swept area (m^2)
c = airfoil chord (m)
c_P = power coefficient
C_A = equivalent chord of the struts (m)
C_D = drag coefficient of the struts (m)
CFD = computational fluid dynamics
D_T = diameter of the central tower (m)
D, H, R = turbine diameter, height, radius (m)
I_{PER} = root mean square of periodic unsteadiness
k = turbulence kinetic energy (m^2/s^2)
N_{BPP} = number of revolutions
N_{PER} = number of samples
P = power (W)
T_{res} = resistant torque of the struts ($\text{N} \cdot \text{m}$)
TSR = tip-speed ratio
V = wind speed (m/s)
V_{PER} = phase-resolved velocity component (m/s)
V_{TM} = time-averaged velocity component (m/s)
VAWT = vertical axis wind turbine
W = relative wind speed (m/s)
X, Y = reference axes
y^+ = dimensionless wall distance

Greek Symbols

θ = azimuthal angle (deg)
ρ = air density ($\text{kg/N} \cdot \text{m}^3$)
ω = specific turbulence dissipation rate (1/s)
ω^* = dimensionless vorticity
Ω = revolution speed of the turbine (rad/s)

Subscripts

0 = value at inlet
$\perp$ = perpendicular direction

References

[1] Paraschivoiu, I., 2002, *Wind Turbine Design With Emphasis on Darrieus Concept*, Polytechnic International Press, Montreal, QC, Canada.
[2] Balduzzi, F., Bianchini, A., Carnevale, E. A., Ferrari, L., and Magnani, S., 2012, "Feasibility Analysis of a Darrieus Vertical-Axis Wind Turbine Installation in the Rooftop of a Building," Appl. Energy, **97**, pp. 921–929.
[3] Borg, M., Shires, A., and Collu, M., 2014, "Offshore Floating Vertical Axis Wind Turbines, Dynamics Modelling State of the Art—Part I: Aerodynamics," Renewable Sustainable Energy Rev., **39**, pp. 1214–1225.
[4] Bianchini, A., Ferrara, G., Ferrari, L., and Magnani, S., 2012, "An Improved Model for the Performance Estimation of an H-Darrieus Wind Turbine in Skewed Flow," Wind Eng., **36**(6), pp. 667–686.
[5] Mertens, S., van Kuik, G., and van Bussel, G., 2003, "Performance of an H-Darrieus in the Skewed Flow on a Roof," ASME J. Sol. Energy Eng., **125**(4), pp. 433–440.
[6] Bianchini, A., Ferrara, G., and Ferrari, L., 2015, "Design Guidelines for H-Darrieus Wind Turbines: Optimization of the Annual Energy Yield," Energy Convers. Manage., **89**, pp. 690–707.
[7] Simão Ferreira, C., Aagaard Madsen, H., Barone, M., Roscher, B., Deglaire, P., and Arduin, I., 2014, "Comparison of Aerodynamic Models for Vertical Axis Wind Turbines," J. Phys.: Conf. Ser., **524**, p. 012125.
[8] Rainbird, J., Bianchini, A., Balduzzi, F., Peiro, J., Graham, J. M. R., Ferrara, G., and Ferrari, L., 2015, "On the Influence of Virtual Camber Effect on Airfoil Polars for Use in Simulations of Darrieus Wind Turbines," Energy Convers. Manage., **106**, pp. 373–384.
[9] Balduzzi, F., Drofelnik, J., Bianchini, A., Ferrara, G., Ferrari, L., and Campobasso, M. S., 2017, "Darrieus Wind Turbine Blade Unsteady Aerodynamics: A Three-Dimensional Navier–Stokes CFD Assessment," Energy, **128**, pp. 550–563.
[10] Balduzzi, F., Bianchini, A., Maleci, R., Ferrara, G., and Ferrari, L., 2016, "Critical Issues in the CFD Simulation of Darrieus Wind Turbines," Renewable Energy, **85**(1), pp. 419–435.
[11] Bianchini, A., Balduzzi, F., Ferrara, G., Ferrari, L., Persico, B., Dossena, V., and Battisti, L., 2017, "A Combined Experimental and Numerical Analysis of the Wake Structure and Performance of a H-Shaped Darrieus Wind Turbine," First Global Power and Propulsion Society Forum, Zurich, Switzerland, Jan. 16–18, pp. 1–8.
[12] Shamsoddin, S., and Porté-Agel, F., 2014, "Large Eddy Simulation of Vertical Axis Wind Turbine Wakes," Energies, **7**(2), pp. 890–912.
[13] Lam, H. F., and Peng, H. Y., 2016, "Study of Wake Characteristics of a Vertical Axis Wind Turbine by Two- and Three-Dimensional Computational Fluid Dynamics Simulations," Renewable Energy, **90**, pp. 386–398.
[14] Dossena, V., Persico, G., Paradiso, B., Battisti, L., Dell'Anna, S., Brighenti, A., and Benini, E., 2015, "An Experimental Study of the Aerodynamics and Performance of a Vertical Axis Wind Turbine in a Confined and Unconfined Environment," ASME J. Energy Resour. Technol., **137**(5), p. 051207.
[15] Persico, G., Dossena, V., Paradiso, B., Battisti, L., Brighenti, A., and Benini, E., 2017, "Time-Resolved Experimental Characterization of the Wakes Shed by H-Shaped and Troposkien Vertical Axis Wind Turbines," ASME J. Energy Resour. Technol., **139**(3), p. 031203.
[16] Bianchini, A., Balduzzi, F., Bachant, P., Ferrara, G., and Ferrari, L., 2017, "Effectiveness of Two-Dimensional CFD Simulations for Darrieus VAWTs: A Combined Numerical and Experimental Assessment," Energy Convers. Manage., **136**, pp. 318–328.
[17] Daróczy, L., Janiga, G., Petrasch, K., Webner, M., and Thévenin, D., 2015, "Comparative Analysis of Turbulence Models for the Aerodynamic Simulation of H-Darrieus Rotors," Energy, **90**(Pt. 1), pp. 680–690.
[18] Maître, T., Amet, E., and Pellone, C., 2013, "Modeling of the Flow in a Darrieus Water Turbine: Wall Grid Refinement Analysis and Comparison With Experiments," Renewable Energy, **51**, pp. 497–512.
[19] Nobile, R., Vahdati, M., Barlow, J. F., and Mewburn-Crook, A., 2014, "Unsteady Flow Simulation of a Vertical Axis Augmented Wind Turbine: A Two-Dimensional Study," J. Wind Eng. Ind. Aerodyn., **125**, pp. 168–179.
[20] ANSYS, 2015, "FLUENT Theory Guide, Release 16.0," ANSYS Inc., Canonsburg, PA.

[21] Balduzzi, F., Bianchini, A., Ferrara, G., and Ferrari, L., 2016, "Dimensionless Numbers for the Assessment of Mesh and Timestep Requirements in CFD Simulations of Darrieus Wind Turbines," Energy, **97**, pp. 246–261.
[22] Balduzzi, F., Bianchini, A., Gigante, F. A., Ferrara, G., Campobasso, M. S., and Ferrari, L., 2015, "Parametric and Comparative Assessment of Navier-Stokes CFD Methodologies for Darrieus Wind Turbine Performance Analysis," ASME Paper No. GT2015-42663.
[23] Bianchini, A., Balduzzi, F., Ferrara, G., and Ferrari, L., 2016, "Influence of the Blade-Spoke Connection Point on the Aerodynamic Performance of Darrieus Wind Turbines," ASME Paper No. GT2016-57667.
[24] Bianchini, A., Balduzzi, F., Rainbird, J., Peiro, J., Graham, J. M. R., Ferrara, G., and Ferrari, L., 2015, "An Experimental and Numerical Assessment of Airfoil Polars for Use in Darrieus Wind Turbines—Part 1: Flow Curvature Effects," ASME J. Eng. Gas Turbines Power, **138**(3), p. 032602.
[25] Menter, F., 1994, "Two-Equation Turbulence-Models for Engineering Applications," AIAA J., **32**(8), pp. 1598–1605.
[26] Amet, E., Maître, T., Pellone, C., and Achard, J.-L., 2009, "2D Numerical Simulations of Blade-Vortex Interaction in a Darrieus Turbine," ASME J. Fluids Eng., **131**(11), p. 111103.
[27] Bianchini, A., Ferrari, L., and Magnani, S., 2011, "Start-Up Behavior of a Three-Bladed H-Darrieus VAWT: Experimental and Numerical Analysis," ASME Paper No. GT2011-45882.
[28] Hoerner, S. F., 1965, *Fluid-Dynamic Drag*, Hoerner Fluid-Dynamics, Bakersfield, CA.
[29] Bachant, P., and Wosnik, M., 2015, "Characterising the Near-Wake of a Cross-Flow Turbine," J. Turbul., **16**(4), pp. 392–410.
[30] Bachant, P., and Wosnik, M., 2015, "UNH-RVAT Baseline Performance and Near-Wake Measurements: Reduced Dataset and Processing Code," figshare, London.